Structural studies of impurity-helium solids

S. I. Kiselev, V. V. Khmelenko, and D. M. Lee
Laboratory of Atomic and Solid State Physics, Cornell University, Ithaca, New York 14853-2501

V. Kiryukhin
Department of Physics and Astronomy, Rutgers University, Piscataway, New Jersey 08854

R. E. Boltnev and E. B. Gordon
Institute of Energy Problems of Chemical Physics, Chernogolovka, 142432, Russia

B. Keimer
Max-Planck-Institute für Festkörperforschung, D-70569 Stuttgart, Germany
(Received 29 August 2001; published 19 December 2001)

We have used x-ray diffraction and ultrasound techniques to study the structure of mesoporous impurity–helium solids created after the injection of impurity particles (D_2, Ne, N_2, Kr) into a volume of superfluid ^{4}He. Clusters of impurities with size of order 50 ± 20 Å and density $\sim 10^{20}$ impurities/cm^3 were observed by x-ray diffraction. The presence of a wide distribution of pore sizes in Im–He solids was revealed by ultrasound (80 to 8600 Å) and by small-angle x-ray scattering (80 to >400 Å). Both x-ray and ultrasound methods detected irreversible structural changes when samples were warmed above $T_\lambda = 2.17$ K. This is ascribed to the aggregation of small clusters caused by thermally activated diffusion. In addition to being of fundamental interest, the properties of the unique porous media studied in this work may be relevant to investigations of low temperature chemical reactions, storage of free radicals, matrix isolation spectroscopy, and superfluid ^{4}He contained in the pores of an extremely compliant medium.

DOI: 10.1103/PhysRevB.65.024517 PACS number(s): 67.40.Yv, 67.40.Mj, 61.10.Eq, 61.46.+w

I. INTRODUCTION

The investigation of nanostructured materials is a rapidly developing research field. A great deal of progress has been achieved in studies of isolated neutral atoms or molecules and nanoclusters of atoms and molecules in liquid and solid helium.[1–4] Studies of the spectral characteristics of single atoms or molecules have provided a great deal of information about the structure of helium surrounding these impurities. The impurities can be divided into two classes according to the sign of the chemical potential inside the helium matrix. It is positive for alkali atoms and electrons and it is negative for most other particles, in particular inert gas atoms and more complex molecules such as D_2 and N_2. Alkali–helium potentials have a more extended repulsive core and a weaker attractive tail than the rare gas–helium potential. Rare gas atoms as well as N_2 and D_2 molecules tend to compress helium atoms in shells around the impurity. It has been suggested by a number of authors that the first two layers of localized helium around a spherical impurity particle can be thought of as a solid in the radial direction but that the helium atoms are relatively free to translate in the azimuthal direction. The same general behavior could be expected for nonspherical particles.[5]

When inert gases or gases such as nitrogen are introduced as impurity particles into liquid helium, we can produce stable impurity–helium (Im–He) clusters, which make it possible to create macroscopic Im–He samples consisting of impurity atoms isolated by localized helium.[6–9] There is the possibility of observing collective effects caused by the interaction between stabilized impurity particles in Im–He samples and also the opportunity to observe chemical reactions in a solid matrix when the behavior of the solid matrix is determined by zero-point motion.[10–12] Introducing the products of a nitrogen–helium radiofrequency discharge into superfluid helium permits production of Im–He samples containing N atoms with relative concentrations unattainable by other techniques. For example, relative concentrations of nitrogen atoms isolated by localized helium ([N]/[He]) in the solid matrix can be as high as approximately 4%.[7,9] The energy density stored in this Im–He sample is comparable to that of chemical explosives.[13]

Macroscopic solid samples formed by injecting impurities into superfluid helium are metastable solid phases built from coalescing clusters of the impurity particles surrounded by solidified helium layers. The preponderance of evidence suggests that aggregates of these clusters are mesoporous solids, similar to extremely porous aerogels. Both are formed by diffusion limited aggregation processes. It is quite reasonable that highly branching structures are formed for the case of Im–He solids. The helium layers surrounding each impurity particle or cluster are expected to be quite thin. They result from the strong van der Waals attractive pressure associated with each impurity particle or cluster. At a sufficiently long distance from the impurity, the effective pressure becomes smaller than the bulk solidification pressure of helium which is greater than 25 atmospheres. Therefore the model of bulk solid helium with embedded impurities does not apply for Im–He solids except under compression. Instead, the close proximity of liquid helium to every impurity or impurity cluster favors a porous branching structure. In recent years superfluid helium in porous materials has been a subject of

 ©2001 The American Physical Society

active theoretical and experimental investigations.[14,15] Finite size effects can shift or smear the superfluid transition in liquid helium. Various porous materials affect the critical behavior of helium near T_λ. Furthermore, sound propagation in superfluid helium has been extensively used in probing the structure of a number of porous materials, including vycor and different porosity aerogels.[16–18] The sound attenuation in liquid helium absorbed in a porous solid reflects the dissipation in the system, and its temperature and frequency dependence is related to the characteristic pore size. The important feature of Im–He solids as compared to other porous materials is that the interaction potential between helium and impurities is well characterized. They also give us a unique opportunity to observe the properties of liquid helium in a porous medium consisting partially of localized helium.

Our previous reports on sound attenuation in helium in Im–He solids point to the presence of a distribution of pore sizes in Im–He samples.[19,20] In the present work we have employed ultrasound propagation and x-ray diffraction to investigate the structural properties of Im–He solids. We have concentrated on molecular impurities such as N_2 and D_2, and inert gas impurities such as Ne and Kr in these experiments. We have found that both x-ray and ultrasound measurements lead to a consistent description of the properties of these solids.

It was determined that Im–He (Im=Ne, N_2) samples consist of the clusters of impurities of order 50 ± 20 Å and characteristic impurity density of $\sim10^{20}$ cm^{-3}. This is consistent with the previous set of x-ray experiments where it was determined that for a freshly prepared Ne-He sample the characteristic size of a constituent building blocks of this porous material is 60 ± 20 Å.[21] This does not rule out the possibility that smaller clusters or single molecules may be present in the sample. In the present work, x-ray measurements monitored the aggregation of the impurities via diffusion during the warming of the sample. X-ray powder patterns of the clusters of impurities were observed as the clusters increased in size during the warming of the sample. Drastic irreversible changes were observed when samples were heated above the T_λ of bulk helium. This is explained by the speeding up of the thermally activated diffusion in that temperature regime because of the poor thermal conductivity of liquid helium.

In a different set of experiments, this process of aggregation of impurities during the warm-up was monitored by sound attenuation measurements using 1, 3, and 5 MHz ultrasound via a pulse time-of-flight technique. Other useful information regarding Im–He solids was also obtained in the ultrasound experiments. For example, the distribution of the pore sizes in the samples was found to be between 80 and 8600 Å. This is consistent with the pore size distribution we obtained from small-angle x-ray scattering in a Ne–He sample, which was determined to range from 80 Å to >400 Å.

II. EXPERIMENTAL METHOD

A. Preparation of porous impurity–helium solids

The technique for creating impurity–helium solids in a volume of superfluid ^{4}He was similar to that developed by the Chernogolovka group.[7,19] A gas jet of helium containing a small fraction (0.5–1 %) of impurity atoms or molecules was directed onto superfluid helium contained in a small dewar beaker sitting in the main helium glass dewar at $T\simeq1.5$ K. The helium vapor pressure in the dewar was maintained at 4–5 Torr by a high speed rotary pump. Figure 1 shows a setup for preparation of Im–He samples in our ultrasound experiments.

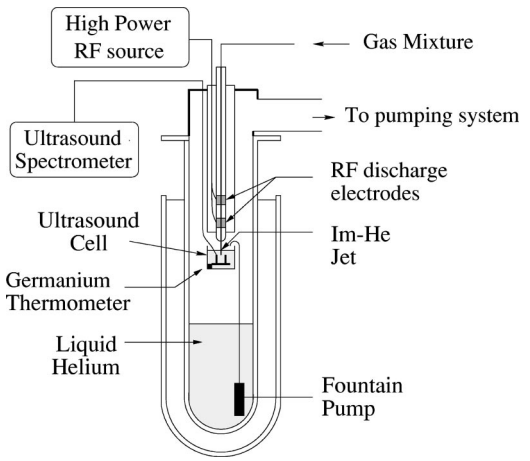

FIG. 1. Experimental setup for preparation of impurity-helium solid samples for ultrasound studies.

The gas entered through a stainless steel capillary with inner diameter of 1.6 mm surrounded by a vacuum jacket with a heater at the bottom end. The diameter of the hole at the end of the capillary was 0.7 mm. The nozzle of the capillary was located 2 cm above the surface of the superfluid helium in the small quartz dewar mentioned above, which acted as the collection beaker. To prevent the freezing of impurities in the nozzle we heated the end of the capillary by an annular heater ($R\simeq10\Omega$). In order to keep the level of helium in the beaker constant, a continuously operating fountain pump was used to transport cold superfluid helium into the beaker from the main liquid helium bath. When the gas mixture jet impinged onto the surface, a macroscopic snowflake-like semitransparent material was created. This fell down through the liquid and then congealed, forming a porous impurity–helium solid in the experimental cell. If free radicals (such as deuterium or nitrogen atoms) were to be studied, a quartz inlet tube with 0.7 mm orifice at the bottom was used to transport the gas sample down to the low temperature region. Near the end of this tube was a high power RF (60 MHz) discharge for dissociation of molecules.

B. Ultrasound experiment

For the case of the ultrasound experiments, the sample was collected between the transducers of the ultrasound cell. The centers of transducers were ~5 cm below the level of helium in the beaker. Two cells of a similar design were used (see Fig. 2). The first one employed *x*-cut quartz crystals (5 MHz fundamental) placed 1.57 cm apart. Each of these was pushed against the parallel walls of the cell by two springs, one of which served as a central electrode. The ground was provided by the brass body of the cell. The second cell used

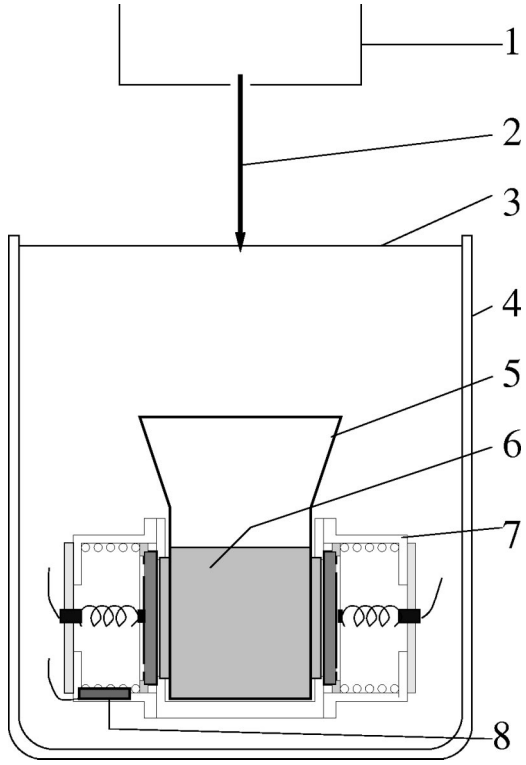

FIG. 2. Experimental cell: 1, Atomic and molecular source; 2, impurity–helium jet; 3, surface of liquid helium; 4, quartz dewar; 5, quartz funnel; 6, impurity–helium solid; 7, ultrasound cell; 8, germanium thermometer (Ref. 20).

$LiNbO_3$ transducers (1 MHz fundamental) placed 1.47 cm apart. For more effective collection of the sample between transducers in the cell, we used a quartz funnel with two side plates which was placed between the endplates of the cell. We could monitor the presence of the sample in the cell and its homogeneity visually through slits on the sides of the glass dewars. In these experiments the impurities used were Ne, Kr and molecular D_2 and/or N_2. Gas mixtures of Im:He=1:100 were used to dilute the impurity particles and therefore prevent them from forming macroscopic impurity granules as they passed from the source to the surface of the liquid helium. The total flux of the gas mixtures was $(4-6)\times 10^{19}$ particles/s. Samples with a visible volume between 1.2 and 1.7 cm^3 were usually employed. In general the samples extended through the entire distance between the transducers.

The ultrasonic measurements were made using a homodyne phase-sensitive spectrometer. A continuously operating oscillator was gated to providing transmitter pulses of 4–12 μs. The amplitude of the input signal could be varied from 1 to 100 V at the resonant frequency or at the odd harmonics of the transmitting crystal. The ultrasonic pulse was received by a receiver crystal, amplified and split in two parts, one of which was used to directly measure the attenuation by recording the amplitude of the signal on a digital oscilloscope. The attenuation was determined by the ratio of the signal voltage U at the receiving transducer to the applied voltage at the transmitter U_0. (We assume a linear relation between the voltage and the vibration amplitudes.) According to the definition of attenuation α,

$$\alpha(\mathrm{dB/cm}) = (20/l)\cdot \log\frac{U_0}{U}, \tag{1}$$

where l is the length of the cell.

The second part of the signal was split again into two parts to obtain the 0° and 90° components, A_{0° and A_{90°. They where used to determine the phase of the signal ϕ:

$$\tan(\phi) = A_{0^\circ}/A_{90^\circ}. \tag{2}$$

Once the initial speed of sound was measured at the temperature T_0 from the pulse transit time τ_0, changes in velocity were calculated from the phase of the received signal,

$$\Delta v = l \Big/ \left(\tau_0 + \frac{\phi(T)-\phi(T_0)}{\omega}\right), \tag{3}$$

where l is the length of the cell. With typical samples the changes in velocity of a few parts per million could be resolved. A second oscilloscope was used to display the signal on a longer time scale. It registered up to 12 echoes of the signal in the first cell but only three echoes in the second one.

For temperature measurements, a calibrated germanium resistor was used. The thermometer was located inside the base of the cell just outside the path of the ultrasonic pulses so that the effect of the temperature difference between the thermometer site and the sound path was minimized. Ultrasound measurements were performed during a slow warmup with a rate of 10^{-4}–10^{-6} K/s. The warmup rate was controlled by constricting the pumping line and was the slowest near the T_λ.

C. X-ray scattering measurements

X-ray scattering measurements were carried out on beamline X20A at the National Synchrotron Light Source at Brookhaven National Laboratory. Im–He samples were produced inside a pumped helium cryostat (T=1.4–300 K) designed for x-ray diffraction measurements. The cryostat was mounted on a two-circle goniometer, and the experiments were performed in a standard horizontal scattering geometry. The energy of x rays was 8 keV. Figure 3 shows a diagram of the insert for a variable temperature cryostat designed for x-ray diffraction measurements. The technique of sample preparation was identical to that used in the ultrasound experiments. The only difference was that the sample was collected in a beryllium can.[21]

After the sample collection was finished, the sample could be maintained in liquid helium at T=1.5–4.2 K, or liquid helium could be drained from the cell. The latter corresponded to a ''dry'' sample. In this case the temperature of the insert could be controlled in the range T=1.5–300 K. For the temperature measurements, we used the same germanium thermometer that was used in the ultrasound experiments. In this case it was placed just outside of the beryllium can (see Fig. 3).

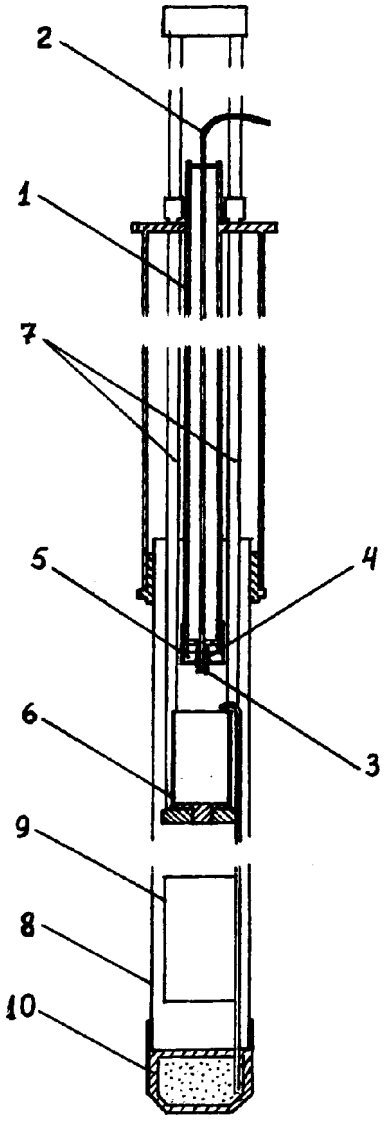

FIG. 3. The diagram of insert for a variable temperature Oxford cryostat: 1, vacuum jacket; 2, capillary; 3, calibrated orifice; 4, heater; 5, dielectric screen; 6, beryllium can with Im–He sample; and germanium thermometer; 7, rods for vertical movement of the can; 8, stainless steel protective tube with a hole for x-ray access (9); 10, fountain pump.

Im–He samples studied in our experiments contained small clusters of impurity atoms with randomly distributed orientations.[21] Therefore, the diffraction patterns produced by these samples are essentially powder diffraction patterns, and standard θ–2θ scans were used for data collection. Momentum transfers from 0.4 Å^{-1} to 2.8 Å^{-1} were accessed. We have also carried out studies at smaller scattering angles, in which data at momentum transfers as small as 0.015 Å^{-1} were collected. For the subsequent data analysis, standard corrections for solid angle, polarization, and sample volume were made. To isolate the scattering due to the Im–He samples from the scattering due to liquid helium, the sample cell, and the cryostat windows, each experiment consisted of two sets of measurements. First, the sample was prepared and x-ray measurements were carried out. Then, the sample was evaporated by heating the sample cell to a high temperature, and the measurements were repeated both for the cell filled with liquid helium, and for the empty cell. The former ''background'' scans were used for the samples immersed in liquid helium, while the latter were used for the ''dry'' samples. These background x-ray scans were subtracted from the Im–He data.

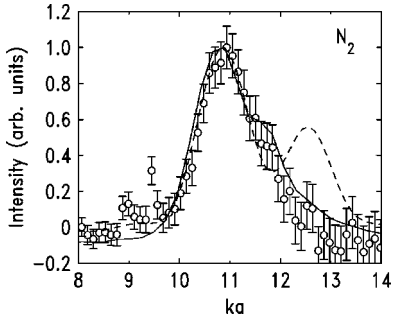

FIG. 4. X-ray diffraction pattern for the N_2–He sample immersed in liquid helium at $T=1.5$ K. Liquid helium signal is subtracted. k is momentum transfer, a is the lattice constant of solid N_2. The solid line is the result of the calculation for 50 Å cluster with four stacking faults, as discussed in the text. The dashed line shows the calculation made for a 30 Å ideal fcc cluster.

III. RESULTS

A. X-ray data and interpretation of x-ray results

In this section, we report x-ray diffraction studies of N_2, Ne, and D_2 impurity–helium solids. In a previous paper,[21] we have reported x-ray studies of Ne samples and preliminary results for the N_2 and Kr samples. Here we extend the investigation of the Ne–He solids to samples prepared under different initial conditions, and also report the results of small-angle scattering experiments. The analysis of the N_2 data is given, and the D_2 samples are briefly discussed.

X-ray diffraction patterns produced by the Im–He samples contain broad diffraction peaks at the Bragg peak positions characteristic of the bulk crystal structure of the pure Im solids. These broad peaks indicate that very small clusters of the impurity atoms are present in our samples.[21]

Figure 4 shows the diffraction data for the N_2–He sample at $T=1.5$ K. Before the data collection, the sample was compressed by heating above T_λ. The sample was surrounded by liquid helium at all times. The liquid helium signal has been subtracted from the data. The data were collected in the vicinity of the (111) and (200) peaks characteristic of cubic solid nitrogen. As in all the x-ray figures shown below, Fig. 4 shows the intensity scattered into the solid angle corresponding to a chosen momentum transfer; corrections for polarization and sample volume were also made. In addition, the intensity is normalized by the division by the square of the atomic factor of nitrogen. The notable features of the data of Fig. 4 are a broad peak at the (111) position ($ka \approx 10.88$), and the *absence* of the peak at the (200) position ($ka \approx 12.57$). As was shown in Ref. 21, this means that

the N_2 clusters in our Im–He samples do not possess the ideal fcc structure of the bulk N_2, but contain a substantial number of defects. This observation is also in agreement with earlier electron diffraction studies of free clusters produced in supersonic jets.[22,23]

In the presence of defects, there is no simple quantitative relation between the width of the diffraction profiles and the cluster size. To determine the typical N_2 cluster size in our samples, we follow the analysis of Ref. 21. We consider fcc clusters containing a specified number of stacking faults, as discussed in Ref. 21. The intensity at the scattering vector k from a collection of such clusters randomly oriented in space is given by the Debye scattering equation[24]

$$I = I_0 \sum_m \sum_n f^2(k) \frac{\sin(kr_{mn})}{kr_{mn}}. \quad (4)$$

Here r_{mn} is the distance between the mth and nth atoms, and $f(k)$ is the atomic form factor of nitrogen. The calculated diffraction patterns were averaged over the different positions of the stacking faults in the cluster.

Model calculations for the N_2–He samples are, in general, more complicated than the calculations for Ne–He samples considered in Ref. 21 because N_2 molecules possess rotational degrees of freedom, and therefore the rotational order of these molecules has to be considered. To address this problem, we have carried out calculations for the ideal fcc clusters using both the actual positions of the nitrogen atoms in the crystal structure, and also in the approximation for which the N_2 molecules were replaced by two nitrogen atoms located at the center of mass of the molecule. The difference between the calculated results in the momentum transfer range of Fig. 4 was much smaller than the experimental errors. Therefore, in the calculations for the clusters with faults, we used the simplified model with two nitrogen atoms located at each point of the corresponding fcc lattice with stacking fault defects.

The best agreement with the experimental data shown in Fig. 4 was obtained for clusters consisting of $\sim$2500 molecules (diameter $\sim$50 Å). The solid line in Fig. 4 shows the calculation made for a cluster with 2352 molecules containing four stacking faults of the deformation type. The dashed line shows the calculation made for an ideal fcc cluster of 450 molecules (diameter $\sim$30 Å). The latter calculation gives the low limit on the cluster size because disordered clusters always produce broader peaks than ideal clusters of the same size. The upper limit on the cluster size can be estimated from the calculation for clusters with random closely packed structure (the number of faults equals the number of closely packed layers). Such calculations averaged over a large number of random distributions of the defects produce a peak width similar to the experimental width for clusters 80 Å in diameter. The agreement with the experimental data in this case, however, is much worse than for the calculation shown in Fig. 4. Therefore, a conservative estimate for the typical cluster size in the N_2 sample of Fig. 4 is 50 ± 20 Å. The minimum number of stacking faults required to explain the experimental data is three.

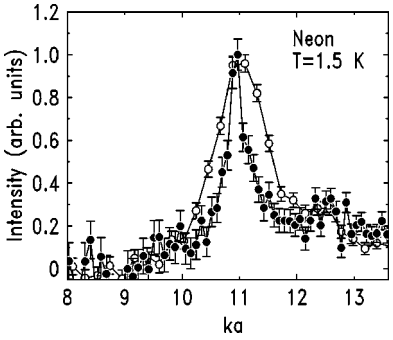

FIG. 5. X-ray diffraction pattern for the different Ne–He samples after preparation in liquid helium at $T = 1.5$ K. Liquid helium signal is subtracted.

There are several sources of systematic errors associated with our determination of the characteristic cluster size of 50 Å. Lattice dynamics effects, for example, were ignored in our calculation. A rough estimate of the Debye–Waller factor based on the Debye temperature of bulk solid nitrogen ($T_\theta \approx 79$ K) indicates that the Debye–Waller correction does not change results of our calculations. However, thermal vibrations in our highly disordered samples in which a substantial fraction of molecules reside near the cluster surfaces are likely to be larger. Another possible source for systematic errors is the restriction of the trial structures to the fcc type. More complex atomic arrangements can, in principle, be realized.

The prevalent cluster size of the N_2 sample discussed above, 50 Å, is similar to the size of the Ne clusters obtained in Ref. 21. The nitrogen atom density of 1×10^{20} cm^{-3} determined from the comparison of the intensities of the nitrogen peaks to the liquid helium signal is also similar to the density of the previously characterized Ne samples. However, samples grown under different preparation conditions exhibited different sample densities as well as different widths of the diffraction peaks. The samples discussed above exhibited some of the broadest peaks that were detected reliably. Samples with significantly broader diffraction peaks, even if successfully prepared, would be undetectable in our experiments because of large experimental errors.

Samples with narrower peaks were, on the other hand, frequently obtained. Figure 5 demonstrates, for example, that neon samples with diffraction peaks 2 times as narrow as the one in Fig. 4 were observed. This corresponds to the neon cluster size roughly twice as large as that obtained from the data of Fig. 4. We conclude that large variations of the prevalent cluster size can be achieved by varying preparation conditions.

The x-ray techniques employed in this work are not able to identify very small clusters or single atoms and molecules in the Im–He solids. Magnetic resonance methods now being developed at Cornell are expected to provide complementary information on these very small units.

Raising the temperature of the sample also results in substantial changes in the sample structure. Figure 6 shows x-ray diffraction patterns for a Ne–He sample at $T = 1.5$ K, and subsequent patterns taken at $T = 4.2$ K. The first pattern at $T = 4.2$ K was taken immediately after the sample was

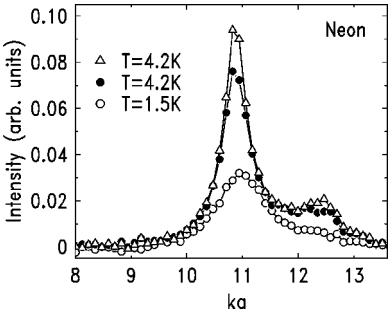

FIG. 6. X-ray diffraction patterns for the Ne–He samples immersed in liquid helium at $T=1.5$ K and $T=4.2$ K. Liquid helium signal is subtracted. k is momentum transfer, a is the lattice constant of solid Ne. The lower curve at $T=4.2$ K was taken immediately after the sample was warmed up. The higher curve at $T=4.2$ K was taken 15 min afterwards.

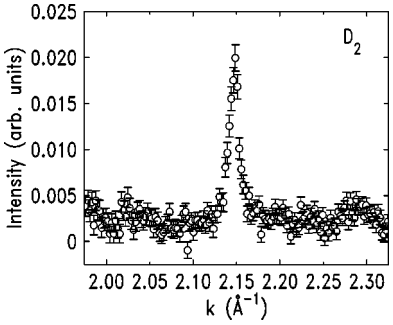

FIG. 7. X-ray diffraction pattern for the D_2 sample at $T=8$ K.

warmed up, and the second pattern was taken ~15 min afterwards. We applied the same corrections as those used for the data of Fig. 4. Increasing temperature results in the growth of intensity and narrowing of the width of the diffraction peaks. The integrated intensity of the cluster peaks grows by a factor of 1.9 as the sample is heated from $T=1.5$ K to $T=4.2$ K, and the intensity increases by another 10% as the sample is kept at $T=4.2$ K for 15 minutes. The integrated intensity is proportional to the total number of atoms in the clusters, and therefore the simplest explanation of its growth is the aggregation of the impurities or clusters of impurities in the Im–He samples as well as macroscopic settling of the suspension. In addition, the shape of the diffraction peaks changes. The changes of the peak shape were attributed in Ref. 21 to the annealing of the lattice defects in the clusters. The model with a fixed cluster size results in lower quality fits to the experimental data at high temperatures (see the top curve in Fig. 3, Ref. 21). Therefore, in all likelihood, the clusters grow with increasing temperature.

We have also attempted to prepare D_2–He samples. In all cases, no detectable diffraction intensity was found immediately after the sample preparation. The absence of a diffraction signal from as-prepared samples most likely results from insufficient data collection times in our experiments; more precise measurements are under way. After heating the sample to $T=4.2$ K in liquid helium, narrow deuterium peaks from macroscopic deuterium particles with fcc structure were always detected. One of these peaks that was observed in a ''dry'' D_2–He solid at $T=8$ K is shown in Fig. 7. The observation of the fcc structure, which is thermodynamically unstable above $T=4$ K, is consistent with previous studies of rapidly cooled deuterium samples.[25] The appearance of narrow peaks in D_2–He solids after warming to 4.2 K indicates the rapid formation of large crystallites. This behavior differs from that of the heavier Im–He solids where the clusters grow in size more gradually.

Finally, we discuss results of small-angle x-ray scattering measurements for the purpose of investigating the possible multiscale behavior of our system. Figure 8 shows the x-ray intensity in a Ne–He sample at $T=1.5$ K where the liquid helium background has been subtracted. As usual, this figure presents the intensity scattered into the solid angle corresponding to a chosen momentum transfer. To interpret these results, we first notice that the Im–He samples most likely contain impurity clusters of a variety of sizes. The fact that no characteristic maxima are observed in the data of Fig. 8 confirms this suggestion. Second, we recall that in multiscale systems with distinct surfaces, such as aerogels and polymers in solutions, the scattered intensity I at small angles often obeys a power law in the magnitude of the scattering vector, k

$$I(k)\sim k^{-d}, \tag{5}$$

where d can vary from 0 to 4.[26,27] For momentum transfers corresponding to length scales smaller than the characteristic size of the building block in the system, $d=4$. For the length scales large enough for the system to be considered uniform, $d=0$. For the intermediate length scales, the value of d depends on the exact microstructure of the system investigated. For the special case of mass fractals, d equals the fractal dimension of the system $(1<d<3)$, and for the case of surface fractals, $d=6-d_s$, where d_s is the surface fractal dimension $(3<d<4)$.

We use Eq. (5) to interpret the small-angle scattering data. For momentum transfers larger than $q\sim 0.08$ Å^{-1}, the $I(k)$ curve appears to follow the k^{-4} law reasonably well, as indicated by the solid line in Fig. 8. This gives the characteristic size of the building block (the impurity cluster) of 80 Å. This number is in reasonable agreement with the typical impurity cluster size estimated above. Because of the small but systematic deviation of the data of Fig. 8 from the

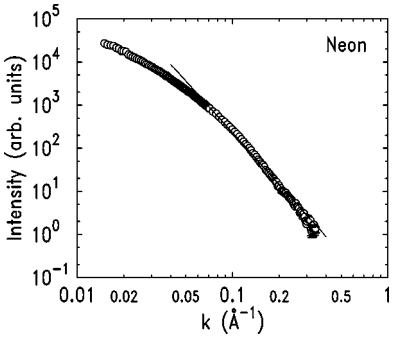

FIG. 8. Small-angle x-ray diffraction pattern for the Ne Im–He sample at $T=1.5$ K. Liquid helium signal is subtracted. The solid line is the fit to the k^{-4} law.

k^{-4} law, it is difficult to determine the exact crossover point, and therefore the error of the estimate of the building block size from the small-angle data is probably significant.

Another important feature of the data shown in Fig. 8 is the absence of saturation ($d=0$ regime) at small values of k. This means that the system is not uniform up to length scales of 400 Å, and therefore pores larger than 400 Å are present in the system.[27] (We can exclude the presence of a significant fraction of impurity clusters of such a large size from data collected at larger momentum transfers, see Fig. 6.) In the intermediate regime ($0.015<k<0.08$), it is tempting to fit the data to Eq. (5) and try to extract the fractal dimension characteristic to our Im–He samples. We note, however, that the range of k accessible in our experiments is not large enough to make a meaningful estimate of d. We leave, therefore, the question of whether our samples possess a fractal structure as a subject of future work.

In summary, the x-ray data described above suggest that the microstructure of the Im–He samples consists of building blocks (impurity clusters) with a distribution of block sizes. The typical building block size in the Ne and N_2 Im–He samples is 50–60 Å. Clusters significantly larger than 100 Å are not present in as-prepared samples. The samples, however, contain a pore distribution from 80 Å to 400 Å in diameter, or even larger. Samples with different densities and different typical block sizes can be grown under different preparation conditions. In particular, Ne clusters with sizes 2 times larger than those described above can be grown. With increasing temperature, the density of the Ne–He and N_2–He samples grows because of the aggregation of impurities as well as because of macroscopic settling of the suspension. The cluster size grows and the cluster structure defects anneal as the temperature increases. These results are further confirmed by the ultrasound measurements described in the next section.

B. Ultrasound data and interpretation

Figure 9 shows the results of 5 MHz ultrasound measurements (in the first cell) at $T=1.1$–2.2 K in different Im–He solids (Im$=D_2$, N_2, Ne, Kr) just after preparation. The attenuation of sound in the presence of Im–He samples (for such heavy impurities as Ne, N_2, Kr) is larger than in bulk helium at low temperatures and increases rapidly with temperature, after which it reaches a plateau and then at the T_λ it goes through a sharp maximum. Whereas heavy Im–He samples all have similar characteristic features, the D_2–He solid behaves quite differently. In the latter case, we do not observe any measurable effect on the speed of sound,[19] and the attenuation has a behavior similar to that of bulk liquid helium, although slightly (~ 1 dB/cm) higher. The samples produced with heavy impurities are much denser than the ones with the D_2 impurity. In the case of the heavy impurities, investigations became impossible above temperature in the neighborhood of 1.4 K because of extremely high attenuation. Therefore, for those samples we were forced to increase the amplitude of the transmitted pulses to very large (up to 100 V) values.

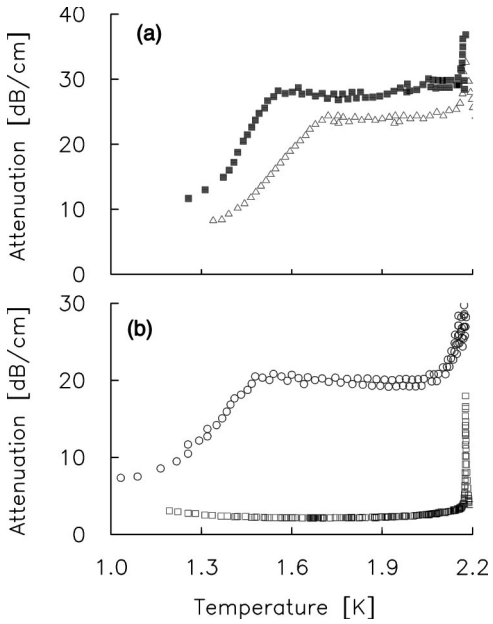

FIG. 9. The behavior of ultrasound attenuation in liquid helium confined in different impurity–helium solids: (a) in Kr–He solid (solid squares), in Ne–He solid (triangles); (b) in N_2–He solid (open circles), in D_2–He solid (open squares).

The characteristic temperature behavior of attenuation in different heavy Im–He samples can be explained by the peculiarities of structure of this porous material, which is characterized by a wide distribution of the pore sizes. Among these pores there are large channels in which the behavior of the helium is close to bulk helium. It is reasonable that these pores should exist, especially if we take into account the method of collecting Im–He solids. This is a highly nonequilibrium process in which the impurity particles cooled by the helium vapor enter the superfluid helium where they stick together after random collisions with each other. So in this process, as the model of aggregation of the small particles into clusters predicts,[28] highly ramified (branching) fractal structures can be created.

The accumulation of Im–He samples is characterized by the existence of a convective flow of helium which moves the pieces of Im–He solid from a location where impurity particles first hit the surface of the helium to the bottom and to the walls of the cell. Later these small pieces of porous material stick together to form the macroscopic Im–He solid. The constituent blocks of these structures are impurity particles and/or clusters of impurity particles encapsulated by one or two shells of localized helium. They could coalesce inhomogeneously, however. Therefore macroscopic voids might be created between them, which can then lead to the formation of large channels in the final sample. We suggest that during the process of injection, impurity atoms and molecules from the gas phase enter superfluid ^{4}He and form loosely connected semirigid network structures. A large volume fraction of this sample is filled with liquid helium. It is possible for any small, isolated impurity–helium clusters with a small number of impurities as a core to be captured inside the rigid structure as they move through the liquid. We

should notice that this Im–He solid preserves its form unless removed from the liquid helium. In this latter case it has been observed visually to compress by up to 60%.[9]

The motion of a fluid in a porous medium during acoustic measurements depends on the pore size and the fluid's properties. Biot created the basic theoretical framework for sound propagation in porous materials.[29] It was successfully applied to ultrasound experiments in superfluid helium in various porous media,[18] including light aerogel. The main parameter used to describe the behavior of sound in liquid in porous materials is the viscous penetration depth

$$\delta_{\mathrm{visc}} = (2\eta/\omega\rho_n)^{1/2}, \tag{6}$$

where η is the viscosity of ^{4}He, ρ_n is the density of the normal component, and ω is the frequency of ultrasound. In superfluid helium the normal fluid fraction changes from almost zero to one between 1.0 K and 2.17 K, causing δ_{visc} to change from 1500 nm to 100 nm for 5 MHz sound. This allows us to give a qualitative explanation of the behavior of the attenuation of sound in Im–He samples, which are thought to be similar to very porous aerogels.

At the lowest temperatures the normal component of helium is locked to the walls of the solid matrix. Therefore the main effect of the fluid is to change the effective density of the porous media and the attenuation is small. Warming leads to a decrease of the viscous penetration depth δ_{visc} as ρ_n increases with temperature so that, when it is comparable to the size R of a particular set of pores (in a distribution of pore sizes), the decoupling of a portion of the normal fluid occurs. During the process of warming up we observed a crossover from the low frequency regime, for which the entire normal component was locked in the pores of Im–He solids to the high frequency regime where more and more normal fluid became unlocked from walls of the pores. Therefore sound attenuation caused by the friction of the layers of normal fluid as they became unlocked from the solid matrix rapidly increases with temperature. Let us call the temperature of this crossover at which attenuation started rapidly increasing T_1. Further warming leads to decoupling of helium in a greater number of pores as smaller and smaller pores begin to play a role with increasing temperature. At a certain temperature the ultrasound waves in those pores become very attenuated and only the sound propagating in the largest channels can be detected. For this case helium is almost like bulk helium and does not feel the effect of the walls, in the sense that most of the liquid is far from the walls. In addition, sound can propagate through the smallest pores formed at the earliest stage of the creation of the sample. Helium in these very small pores is still locked to the solid matrix and attenuation is low and almost independent of temperature. The above considerations lead to the behavior of attenuation resembling that in bulk liquid helium, meaning that attenuation is almost independent of temperature. Let us call this temperature, at which attenuation reaches a plateau, T_2 (Figs. 9, 10).

By calculating viscous penetration depths for T_1 and T_2, we can find the corresponding pore size ($R \simeq \delta_{\mathrm{visc}}$). These results, inferred from Fig. 9, are shown in Table I. Samples

TABLE I. Values of T_1 and T_2 (see text) for different Im–He solids and corresponding pore sizes R. Note that calculations of R can also be performed for temperatures intermediate between T_1 and T_2.

Sample	T_1 (K)	R_1 (nm)	T_2 (K)	R_2 (nm)
Kr–He	1.2	530	1.56	210
Ne–He	1.35	320	1.73	150
N_2–He	1.1	860	1.58	240

produced by injecting heavy impurities in superfluid helium are characterized by the presence of pores of large size–from 150 nm to 860 nm. It should be pointed out that from the analysis of the low temperature part of attenuation, we can estimate sizes only for pores of larger diameter in the case where increasing attenuation is observed. Information about the smallest pores is much harder to obtain because above T_2 where unlocking would take place, sound propagates not only through these small pores but also through helium in the large size channels.

This model is supported by investigations of sound attenuation in the N_2–He sample but at different sound frequencies (Fig. 10). A decrease in frequency leads to a decrease of attenuation for the pores[18] as well as for the large channels where bulk behavior is expected. The smaller the frequency, the larger the viscous penetration depth, according to Eq. (6), which leads to more normal fluid being locked and lower attenuation. T_1 corresponds to the temperature where unlocking starts to occur in the largest pores. T_2 corresponds to the temperature where domination by the large channels and the very smallest pores takes effect. There will be a distribution of pore sizes, but unlocking occurs for a given pore size R when $\delta_{\mathrm{visc}} \sim R$, where δ_{visc} is given by Eq. (6). Note from this equation that the temperature dependence of δ_{visc} is via ρ_n and η. We have calculated the value of δ_{visc} from Fig. 10 at T_2 for each of the frequencies ($T_2 = 1.6$ K at 3 MHz and $T_2 = 1.48$ K at 5 MHz) and find that they are

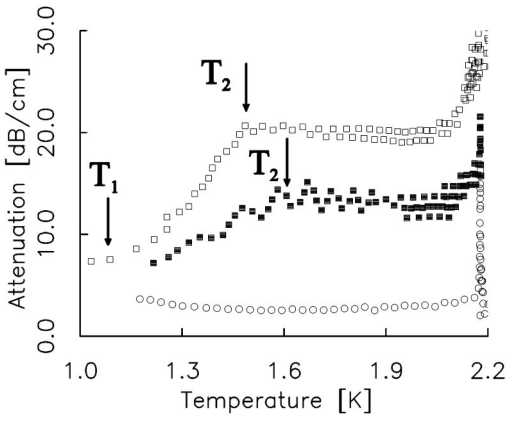

FIG. 10. The behavior of ultrasound attenuation in liquid helium: in bulk (open circles) and confined in N_2–He solid at 3.16 MHz (solid squares), at 5.33 MHz (open squares). The attenuation oscillations here and in other similar data are not understood. See Ref. 20.

both equal to 240 nm. Note that for a given value of $R \sim \delta_{\mathrm{visc}}$, T_2 will occur at a higher temperature for the lower frequency (3 MHz) as can be seen by equating the right-hand sides of Eq. (6) for the two frequencies. Note that T_2 for the ultrasound data at 3 MHz is slightly obscured by small attenuation oscillations, which are not presently understood. A similar comparison was not possible for the case of T_1 because T_1 is not well defined in the 3 MHz data.

Im–He samples formed in our experiments have a variety of different ratios between the volumes of the porous part and the large channels. Compressing these samples leads to a decrease in the volume of the large channels, which in turn increases the attenuation, as was detected in previous experiments.[19]

Analysis of sound propagation in Im–He solids thus shows a distribution of the sizes of channels containing superfluid helium, including very large channels, in which the helium behavior is close to that of bulk helium. The approach used above can only give information about the presence of relatively large pores with size comparable to the viscous penetration depth at temperatures between 1.1 and 2.17 K. In order to obtain information about the smallest pores in which normal helium is locked to the surface of Im–He solid through most of the temperature range investigated, we determined the width of the attenuation peak near the λ point. This attenuation peak corresponds to the destruction of superfluidity in the smallest pores in the immediate neighborhood of the λ point. The onset of this peak occurs when the correlation length in helium becomes comparable to the pore size. Josephson's relation[30] for helium gives the temperature dependence of the correlation length in helium near T_λ:

$$\xi(t) = \xi_0 |t|^{-\zeta} = \frac{k_B T_c m^2}{\hbar^2 \rho_s(t)}, \tag{7}$$

where m, k_B, and $\hbar$ are the mass of a helium atom, Boltzmann's constant and Planck's constant, respectively. From Fig. 9 we can say that the onset of broadening of the attenuation peak for the N_2–He sample studied is at $T \simeq 2.1$ K, which gives the characteristic size of the pores from the argument above as ~ 80 Å. This is reasonably close to 50 ± 20 Å, the size of the clusters from which our Im–He solids are built, as obtained from x-ray studies.

Under certain favorable circumstances we were able to produce D_2–N_2–He samples without any of the large channels and in this case we did not observe the plateau in the temperature dependence of the attenuation.[20] We are planning further investigations of this phenomenon.

Now we shall discuss the factors affecting the structural stability of Im–He samples. Changes in the structure should lead to changes in the attenuation of ultrasound. The comparison of attenuation in freshly prepared samples and in those cycled above T_λ showed that crossing the λ transition always gives a somewhat larger attenuation.

Figure 11(a) displays the sound attenuation in a N_2–He solid. Here we observed a very pronounced effect of increase of attenuation after the sample is cycled above the λ point. In contrast, warming the samples to temperatures slightly *below* the λ point and cooling them down again did not lead to any observable changes in attenuation of sound. This allows us to conclude that structural changes take place primarily after heating the samples *above* the λ point, where liquid helium does not have a thermal conductivity high enough to serve as a thermal bath to smooth out the local temperature variations caused by recombination of atoms (a large effect) or by associations of molecules of impurities (a smaller effect).

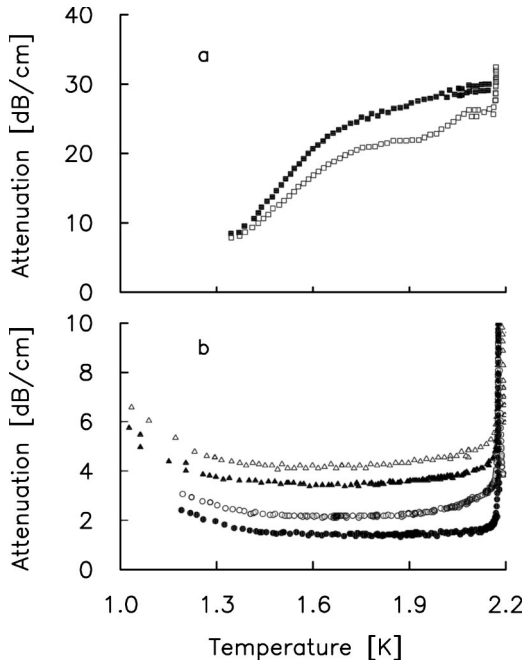

FIG. 11. The attenuation of ultrasound in liquid helium: (a) in N_2–He solids [after preparation (open squares), after crossing λ point and cooling down (solid squares)]; (b) in bulk helium (solid circles), in D_2–He and D–D_2–He solids [after preparation of both solids (open circles)], after crossing λ point and cooling down D_2–He (solid triangles), after crossing λ point and cooling down D–D_2–He (open triangles).

Figure 11(b) shows the attenuation of sound in fresh D–D_2–He and in D_2–He samples which were later cycled above the λ point. The former sample, which contains D atoms, was prepared with an RF discharge. The attenuation of sound in both of these fresh samples was identical. Warming samples above the λ point and cooling them down led to a slight increase of attenuation by ~ 2 dB and ~ 1.35 dB for D–D_2–He and D_2–He, respectively, but the characteristic behavior of attenuation did not change (it was still similar to that in pure helium).

The difference in change of attenuation in D–D_2–He and D_2–He samples can be explained by the occurrence of recombination of stabilized D atoms which releases ~ 4.5 eV per each recombination. This is much greater than the heat of aggregation associated with van der Waals forces between deuterium molecules. Therefore the heat of recombination of D atoms may initiate and accelerate the thermal diffusion of neighboring deuterium atoms and molecules. This leads to association of neighboring impurity particles and creation of regions with a larger concentration of Im–He sample thereby

leading to increased attenuation. This is similar to the effect observed in the heavier Im–He solids.

The difference of the characteristic behavior of sound attenuation in D_2–He and heavier Im–He samples can be explained by the difference in rigidity of these samples. Only in the case of heavier impurities is it possible, as a result of larger Im–Im and Im–He van der Waals interactions, to create a rather rigid, although still somewhat compliant, porous structure. That is why we observe the additional attenuation due to sloshing of the normal component of helium relative to the normal helium viscously clamped to the semirigid porous network. In the case of deuterium impurities, van der Waals forces associated with the D_2–D_2 and D_2–He interactions are much smaller and closer to the He–He interaction. As a result very compliant D_2–He solids can be formed in the superfluid helium. In fact, zero point energy plays a major role in determining the properties of Im–He solids containing the lightest impurities. Hence these Im–He solids involving light impurities are quantum solids. The small increase of sound attenuation in D_2–He samples compared with bulk helium can be explained by an increase in the effective density of the medium compared with pure bulk helium. But there is no clear evidence of viscous losses in the surface layers of liquid helium in the sample pores in this case, as opposed to results in the Im–He solids involving the heavier impurities.

Finally, we consider the behavior of the sound attenuation in helium in Im–He solids near the λ point. The results of measurements of attenuation near the T_λ for Im–He samples (Im=Ne, N_2, Kr) shows that the maxima of attenuation near the λ point for these samples are much broader than for liquid helium (see Figs. 9 and 10), making the precise determination of the position of the maxima impossible. We can conclude from this data that there is no significant shift of the λ point for helium-filled porous heavy Im–He solids.

On the other hand, Fig. 12 shows the behavior of the velocity and attenuation of ultrasound (only 5 MHz data is presented) in the mixed D_2–N_2–He solids. The width of attenuation peak near λ point is only slightly broader than for pure helium. That makes it possible to determine the more precise position of the center of the peak. It appears that the shift of peak with respect to bulk helium is ~ 0.2 mK, but at the same time the reproducibility of the measurements of the sound attenuation maximum in liquid helium from run to run is about ~ 0.1 mK. Therefore based on these experiments we can say that the shift in the onset of superfluidy in D_2–N_2–He solids is on the order of 0.2 mK, which is similar to that for a very light aerogel (~ 0.3 mK in 0.5% dense silica arogel[15]). Note that Fig. 12 reflects the fact that the attenuation peak in bulk helium is ~ 0.08 mK below the λ point.[31]

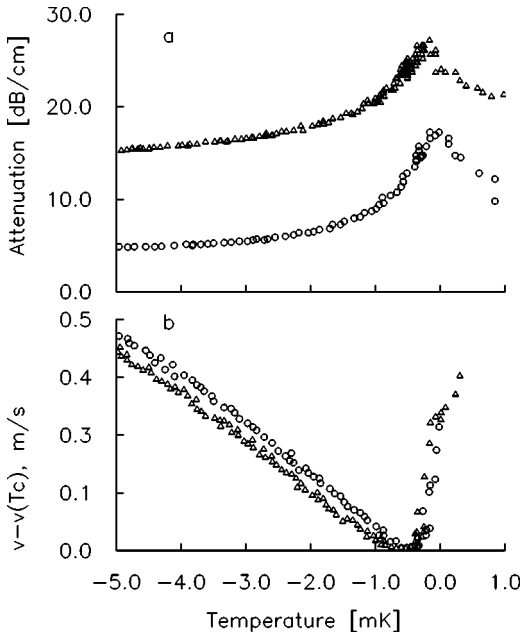

FIG. 12. The behavior of attenuation (a) and velocity (b) of ultrasound in liquid helium near λ point: in bulk (open circles), in D_2–N_2–He solid (open triangles). For the D_2–N_2–He solid the attenuation is shifted up by 10 dB/cm.

IV. DISCUSSION AND CONCLUSION.

Im–He solids have opened up a variety of intriguing possibilities for experimental investigations of the quantum properties of helium, as well as for studying atoms, molecules and small clusters stabilized in solidified helium. These studies provide a new perspective for matrix isolation in solidified helium. The big advantage of the Im–He solids is that a large variety of atoms or molecules can be used to build the ''backbone'' of the Im–He samples. It also appears that, depending on the preparation conditions, samples with different nanostructures can be prepared. To understand the properties of the Im–He samples it is necessary to determine their microscopic structure.

In the present work, we have been investigating the structure of the porous Im–He solids by means of ultrasound propagation through liquid helium contained in the pores and via x-ray diffraction studies. Upon the introduction of impurity particles in superfluid helium the single impurities or small clusters of impurities surrounded by a couple of layers of localized helium play a dominant role. The early ESR and optical spectroscopy data[7,10] are consistent with this idea. These small Im–He clusters are believed to be assembled into a highly porous structure consisting of clumps connected by strands. If the impurity clusters are very close to one another, then a fairly rigid structure might exist. This porous structure would then have some features in common with aerogel, which has been extensively used in the studies of superfluid helium in constricted geometries. Our analysis of the x-ray and ultrasound data in this work is consistent with the above description. We found that the heavier impurities (Ne, N_2, Kr) tend to create clusters of order 50 ± 20 Å to form mesoporous material with an estimated impurity density $\sim 10^{20}$ cm^{-3}. In our ultrasound experiments a wide distribution of the pore sizes from 80 to 8600 Å were observed. This data was confirmed by small-angle x-ray scattering, where we established the presence of the pores from 80 Å to >400 Å.

Irreversible changes in attenuation upon heating of Im–He samples and in diffraction patterns during the warm-

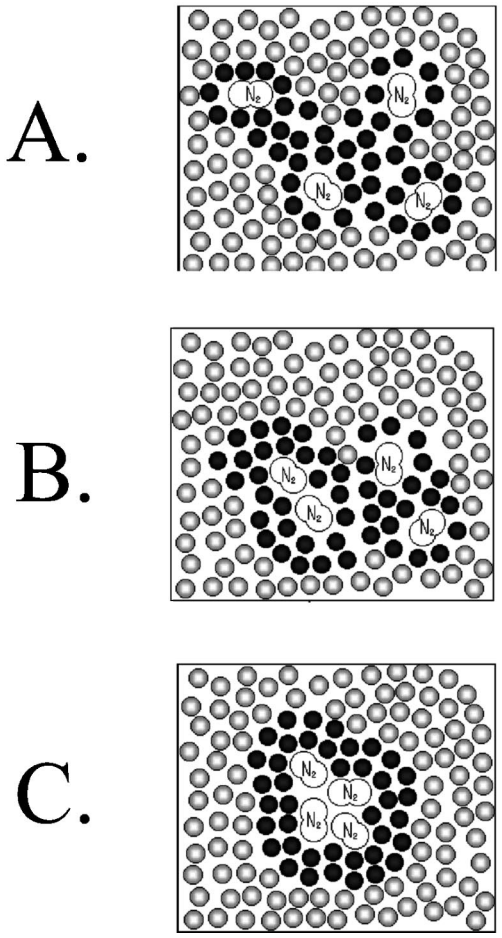

FIG. 13. The model of Im–He solid formation: (A). On formation, the impurities are mainly isolated from one another by helium atoms in the solid (black circles). Superfluid liquid helium contained in the pores (gray circles) transports heat efficiently. (B) As the sample is warmed up, diffusion allows impurities to aggregate slowly. The associated heat is carried away by superfluid helium. (C). As the sample is warmed above the T_λ, the diffusion rate increases. Larger aggregates form. The heat of aggregation can no longer be carried away by liquid helium for $T > T_\lambda$. More diffusion takes place and even larger aggregates form.

ing above T_λ are attributed to thermal diffusion: As the samples warm, thermal diffusion of helium atoms in the surrounding coatings and of the impurities themselves speeds up. The impurity clusters slowly grow in size. This effect is enhanced by release of the heat of aggregation of the impurity clusters. This effect has also been studied by optical spectroscopy below T_λ.[10] A dramatic increase in the growth rate of the impurity clusters is expected to occur for temperatures above the superfluid transition T_λ because the thermal conductivity of liquid helium in the pores becomes dramatically smaller as the sample is heated through T_λ. Thus the heat of aggregation can lead to local hot spots which contribute to higher diffusion rates in these localized regions, a situation which is favorable to the formation of larger impurity clusters. It is therefore to be expected from this crude model that heating the sample above T_λ and then cooling back would lead to irreversible behavior. This is exactly what has been observed in the present work. The expected time evolution according to this model for a sample is shown schematically in Fig. 13.

For the case of atomic free radical impurities, the very large amount of heat released during molecular recombination enhances the effects described above. For very high concentrations of free radicals, the sample will spontaneously explode. Theoretical studies of the stability of atomic free radicals (such as N atoms) in a molecular solid (N_2) were reviewed by Jackson many years ago.[32] A static statistical theory showed that radical concentrations up to 10% were possible. On the other hand, a dynamical statistical theory involving chain reactions gave maximum concentrations of N in solid N_2 of less than 0.1%. Further analysis of thermal stability of small specimens (size <1 μm) of molecular nitrogen which contain trapped nitrogen atoms gave an upper limit of 1% for concentration of N atoms.[33] The Im–He solids greatly exceed this latter limit, as mentioned above.

The importance of this work is that it shows quite clearly the necessity of maintaining the impurity–helium solids at temperatures below the lambda temperature to prevent excessive recombination for the free radical impurities and also to prevent structural changes in all samples. This is especially significant for purposes of any applications requiring energy storage.

The work described herein provides new opportunities to explore various types of interesting behavior for a new set of porous materials. For example, the superfluid transition of helium can be studied within the constrained geometries of the impurity–helium solids. We observed a definite broadening in the λ peak in measurements of sound attenuation vs temperature. This broadening increases with increasing sample density. A small shift of the λ transition temperature ($\Delta T \sim 0.2$ mK) was first noted for D_2–N_2–He samples.

ACKNOWLEDGMENTS

We would like to thank NASA for its support through grant NAG 8-1445. This work was also supported by A.P. Sloan Foundation (V.K.), RFBR grant 99-03-33261 (R.E.B.) and Leading Scientific Group Support grant 00-15-97400 (E.B.G.). We also wish to thank John Beamish, Drew Geller, Gavin Lawes, Jeevak Parpia, and John Reppy for very useful suggestions and discussions.

[1] B. Tabbert, H. Gunter, and G. zu Putlits, J. Low Temp. Phys. **109**, 653 (1997).
[2] J.P. Toennies and A.F. Vilesov, Annu. Rev. Phys. Chem. **49**, 1 (1998).
[3] S.I. Kanorsky and A. Weis, Adv. At., Mol., Opt. Phys. **38**, 87 (1998).
[4] E.B. Gordon, A.F. Shestakov, Low Temp. Phys. **26**, 1 (2000).
[5] Y. Kwon, P. Huang, M.V. Patel, D. Blume, and K.B. Whaley,

Chem. Phys. **113**, 6469 (2000); Y. Kwon, D.M. Ceperley, and K.B. Whaley, *ibid.* **104**, 2341 (1996); F. Dalfovo, Z. Phys. D: At., Mol. Clusters **29**, 61 (1994).
[6] E.B. Gordon, A.A. Pelmenev, O.F. Pugachev, and V.V. Khmelenko, JETP Lett. **37**, 282 (1983).
[7] E.B. Gordon, V.V. Khmelenko, E.A. Popov, A.A. Pelmenev, and O.F. Pugachev, Chem. Phys. Lett. **155**, 301 (1989).
[8] E.B. Gordon, V.V. Khmelenko, A.A. Pelmenev, E.A. Popov, O.F. Pugachev, and A.F. Shestakov, Chem. Phys. **170**, 411 (1993).
[9] R.E. Boltnev, E.B. Gordon, I.N. Krushinskaya, A.A. Pelmenev, E.A. Popov, O.F. Pugachev, and V.V. Khmelenko, Sov. J. Low Temp. Phys. **18**, 576 (1992).
[10] R.E. Boltnev, E.B. Gordon, V.V. Khmelenko, I.N. Krushinskaya, M.V. Martynenko, A.A. Pelmenev, E.A. Popov, and A.F. Shestakov, Chem. Phys. **189**, 367 (1994).
[11] R.E. Boltnev, E.B. Gordon, I.N. Krushinskaya, M.V. Martynenko, A.A. Pelmenev, E.A. Popov, and V.V. Khmelenko, Low Temp. Phys. **23**, 567 (1997).
[12] R.E. Boltnev, I.N. Krushinskaya, A.A. Pelmenev, D.Yu. Stolyarov, and V.V. Khmelenko, Chem. Phys. Lett. **305**, 217 (1999).
[13] B. Palaszewski, L.S. Ianovski, and Patrick Carrik, J. Propul. Power **14**, 641 (1998).
[14] J.D. Reppy, J. Low Temp. Phys. **87**, 205 (1992); L.S. Goldner, N. Mulders, and G. Ahlers, *ibid.* **93**, 131 (1993).
[15] J. Yoon, D. Sergatskov, J. Ma, N. Mulders, and M.H.W. Chan, Phys. Rev. Lett. **80**, 1461 (1998).
[16] K.L. Warner and J.R. Beamish, Phys. Rev. B **36**, 5698 (1987).
[17] N. Mulders and J.R. Beamish, Phys. Rev. Lett. **62**, 438 (1989).
[18] K. Warner and J.R. Beamish, Phys. Rev. B **50**, 15 896 (1994).
[19] S.I. Kiselev, V.V. Khmelenko, D.A. Geller, J.R. Beamish, and D.M. Lee, J. Low Temp. Phys. **119**, 357 (2000).
[20] S.I. Kiselev, V.V. Khmelenko, and D.M. Lee, Low Temp. Phys. **26**, 641 (2000).
[21] V. Kiryukhin, B. Keimer, R.E. Boltnev, V.V. Khmelenko, and E.B. Gordon, Phys. Rev. Lett. **79**, 1774 (1997).
[22] G. Torchet, J. Farges, M. F. de Feraudy, and B. Raoult, in *The Chemical Physics of Atomic and Molecular Clusters*, edited by G. Scoles (North-Holland, New York, 1990), pp. 513–542.
[23] S.I. Kovalenko, D.D. Solnyshkin, E.T. Verkhovtseva, and V.V. Eremenko, Chem. Phys. Lett. **250**, 309 (1996).
[24] B.E. Warren, *X-ray Diffraction* (Addison-Wesley, Reading, MA, 1969).
[25] J.L. Yarnell, R.L. Mills, and A.F. Schouch, Sov. J. Low Temp. Phys. **1**, 366 (1975).
[26] D.W. Schaefer and K.D. Keefer, Mater. Res. Soc. Symp. Proc. **32**, 1 (1984). H.D. Bale, and P.W. Schmidt, Phys. Rev. Lett. **53**, 596 (1984).
[27] D.W. Schaefer and K.D. Keefer, Phys. Rev. Lett. **56**, 2199 (1986).
[28] P. Meakin, Annu. Rev. Phys. Chem. **39**, 237 (1988).
[29] M.A. Biot, J. Am. Chem. Soc. **28**, 168 (1956); **28**, 179 (1956).
[30] B.D. Josephson, Phys. Lett. **21**, 608 (1966).
[31] C.E. Chase, Phys. Fluids **1**, 3 (1958).
[32] J.L. Jackson, *Formation and Trapping of Free Radicals*, edited by A.M. Bass, and H.P. Broida (Academic, New York and London, 1960), p. 327.
[33] E.B. Gordon, L.P. Mezhov-Deglin, O.F. Pugachev, and V.V. Khmelenko, Sov. Phys. JETP **46**, 502 (1977).